Available online at www.sciencedirect.com

SciVerse ScienceDirect

Ceramics International 38 (2012) 4201–4208

CERAMICS INTERNATIONAL

www.elsevier.com/locate/ceramint

Characterization of Mg doped ZnO nanocrystallites prepared via electrospinning

Saime Sebnem Cetin [a,*], Ibrahim Uslu [b], Arda Aytimur [b], Suleyman Ozcelik [a]

[a] Gazi University, Faculty of Science, Teknikokullar, Ankara 06500, Turkey
[b] Gazi University, Gazi Faculty of Education, Teknikokullar, Ankara 06500, Turkey

Received 14 September 2011; received in revised form 30 January 2012; accepted 1 February 2012
Available online 9 February 2012

Abstract

Undoped and Mg doped ZnO nanofibers with different doping concentrations were successfully synthesized using the electrospinning technique. The nanofiber structures were calcined at 300 °C, 400 °C, 500 °C, and 600 °C respectively. It was observed that the nanofibers turned into a nanoparticular structure at the calcining temperature of 400 °C. The nanoceramic mats were characterized by the Fourier transform infrared-attenuated total reflectance spectroscopy and by the scanning electron microscopy. The electronic band transitions of as-deposited and calcined films were identified by the evaluation of the photoluminescence measurements at room temperature. It was observed that the exitonic transition energy of the ZnO nanostructure blue-shifted to a high energy value with an increasing Mg doping ratio. In order to estimate the decomposition temperature of the nanofibers turning into a nanoparticular structure, the nanofiber structure was calcined at temperatures between 300 °C and 400 °C, the temperature ramp being 20 °C. The evaluation of the emission spectra of the calcined structures show that the decomposition of electrospun nanofibers started at 320 °C. In addition, band gap energies of the samples were determined by the transmittance measurement of the samples and by the UV–VIS spectrophotometer at the room temperature.

Keywords: A. Calcination; C. Optical properties; D. ZnO; D. MgO

1. Introduction

Zinc oxide (ZnO) structures have excellent electronic and optical properties such as a large exciton binding energy (i.e. 60 meV), and a large band gap energy (3.37 eV at room temperature) with a variety of applications including catalysts, gas sensors, thin film-based electronic and electro-optic devices, and varistors [1–6]. Metal acetates such as zinc acetate and magnesium acetate are useful reagents in the organic synthesis of metal oxide nanostructures [7,8,10–12]. A small amount of dopant metal oxide materials such as MgO, Bi_2O_3, Co_3O_4, MnO, Sb_2O_3, Cr_2O_3 and so on are the main tools to produce ZnO alloys with a higher band-gap for possible quantum well structures [13,14]. Mg has been chosen as a dopant because a large number of reports indicate the enhancement of the band gap of the ZnO by doping it with different concentrations of Mg [7]. Currently, there are many methods used to prepare ZnO nanomaterials and nanofibers such as electrospinning [10,15], sol–gel [8,9,16], sputtering [17,18], and chemical vapour deposition [19]. The electrospinning technique has been preferred because of its simplicity and low cost [10].

In this study, the synthesis of Mg doped zinc oxide nanoparticles has been carried out using the electrospinning technique. ZnO samples were calcined at different temperatures by conventional thermal annealing (CTA) in air atmosphere. The surface morphology of the films depending on the calcination temperature was characterized by scanning electron microscopy (SEM) measurements. Chemical bonding structures in the samples were investigated using a Fourier transform infrared-attenuated total reflectance spectroscopy (FTIR-ATR) The effect of the Mg content on the electronic band transitions in the prepared structures were investigated by photoluminescence (PL) spectra at room temperature. In addition, the band

* Corresponding author at: Gazi University, Faculty of Science, Department of Physics, Teknikokullar, 06500 Ankara, Turkey. Tel.: +90 312 2021268; fax: +90 312 2122279.
E-mail address: cetins@gazi.edu.tr (S.S. Cetin).

0272-8842/$36.00
doi:10.1016/j.ceramint.2012.02.003

gap of the samples was determined by the transmittance measurement of the samples by an UV–VIS spectrophotometer at room temperature.

2. Experimental

2.1. Materials and method

In the experiments, PVA (average M_w of 85,000–124,000) was obtained from Sigma Aldrich, zinc acetate and magnesium acetate were obtained from Merck and ultrapure deionized water was used as a solvent.

The experimental procedure of this study consists of three major steps: (i) the preparation of the metal acetate composite precursor polymeric solution. (ii) The electrospinning of the composite precursor polymeric solution to generate composite nanofibers consisting of matrix polymer and precursor (zinc acetate, magnesium acetate and PVA). The spinning experiments are usually performed at room temperature. (iii) The calcination or the chemical conversion of the precursor polymeric nanofibers into the desired ceramic at an elevated temperature, with concomitant removal of all organic components from the precursor nanofibers.

2.2. Preparation of the composite precursor polymeric solution

The aqueous PVA solution (10%) was first prepared by dissolving the PVA powder in ultra pure distilled water and heating it to 80 °C, stirring it for 3 h and then cooling it to room temperature while continuously stirring it for 2 more hours. Four hybrid polymer solutions were prepared as follows: 2 g of zinc acetate and 0.04 g of magnesium acetate were added drop by drop into a 40 g aqueous PVA at 60 °C separately, and each hybrid polymer solutions were stirred vigorously using a magnetic stirring bar for 3 h at this temperature. As a final product, viscous gels of the PVA/Zn–Mg acetate hybrid polymer solutions were obtained.

2.3. The electrospinning of the solution and calcinations of the samples

The hybrid polymer solutions were poured in syringes, the needle (18 gauge) being connected to the positive terminal of a high-voltage supply (Gamma High Voltage Research) which was able to generate DC voltages up to 40 kV. The suspension was delivered to the needle by a syringe pump (New Era Pump Systems Inc., USA). The distance between the tip of the needle and the aluminum collector (glass slides) was fixed at 21 cm. The following operative parameters were chosen: a flow rate of 0.4 ml/h and an applied voltage of 25 kV. Thus the glass slides were coated with magnesium doped zinc nanofibers. The fibers formed as a result were dried in vacuum for 12 h at 80 °C.

One part of the glass slides containing nanofibers was calcined for 3 h at four different temperatures, 300 °C, 400 °C, 500 °C, and 600 °C at atmospheric conditions to obtain the magnesium doped zinc oxide nanostructure. In addition, the nanofiber structure was calcined at different temperatures between 300 °C and 400 °C with a rump of 20 °C with the aim of determining the decomposition temperature of the nanofibers to the nanoparticle structure. The entire calcining process was performed by conventional furnace in air. Heating and cooling rate for all calcinations process was fixed at 8 °C/min.

2.4. Measurement and characterization

The pH and electrical conductivity of the hybrid polymer solutions were measured using the Wissenschaftlich-Technische-Werkstätten WTW and the 315i/SET apparatus. The viscosity of the hybrid polymer solutions was measured using an AND SV-10 viscometer.

Fiber morphology, average fiber diameter and distribution were determined by a scanning electron microscopy (JEOL JSM 7000 F Field Emission) on samples sputtered with gold and observed at an accelerating voltage of 10 kV. Fiber diameter was measured by the image processing software called ImageJ (Image Pro-Express, Version 5.0.1.26, and Media Cybernetics Inc.). ImageJ is a public domain Java image processing program [20]. Also, the topographic changes of the ZnO samples depending on calcination temperature were characterized by SEM measurements. In addition, the PL measurements were performed by using the Jobin Yuvon Florog-550 system with a 50 mW He-Cd laser (λ = 325 nm) as an excitation light source at room temperature. The transmittance measurements were examined with a Perkin Elmer 45 UV–VIS spectrophotometer, the wavelength ranging from 200 nm to 1100 nm. The absorbance spectra were recorded by using a Bruker-880 FTIR-ATR spectrometer.

3. Results and discussion

The pH, the viscosity and the electrical conductivity of the PVA, zinc and magnesium acetate composite precursor polymeric solution was measured before the electrospinning experiment. The obtained parameters are given in Table 1. The undoped and the Mg doped ZnO nanofibers with the ratio of

Table 1
Physical properties of the polymer solutions.

Polymer solution	Solution #	Electrical conductivity (mS/cm)	Viscosity (Pa s)	pH
PVA/Zn acetate	1	7.370	0.471	3.26
PVA/(Zn–%2 Mg) acetate	2	7.740	0.605	3.98
PVA/(Zn–%4 Mg) acetate	3	7.780	0.665	3.98
PVA/(Zn–%6 Mg) acetate	4	8.020	0.672	3.91

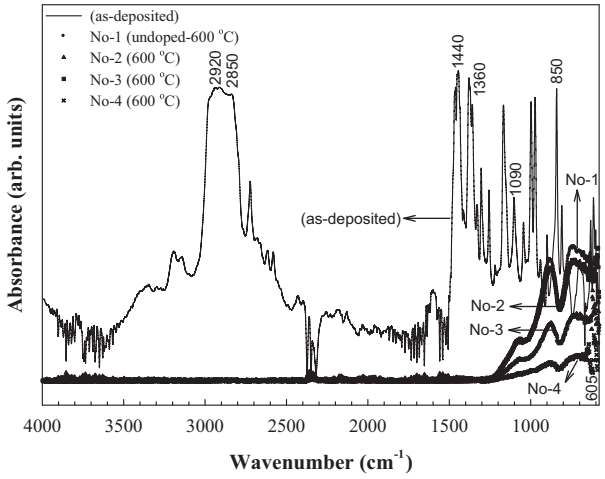

Fig. 1. FTIR-ATR absorbency spectra of the electrospun fibers of PVA/Zinc acetate magnesium acetate nanofibers and calcined undoped and Mg doped ZnO samples at 600 °C.

2%, 4% and 6% are named with No: 1, 2, 3 and 4, respectively. The addition of metal acetates increased the pH, viscosity and the electrical conductivity of the precursor polymeric solution as expected. The pH increased due to composition of the acetate buffer. If metal acetates are added to the solution, hydronium (H_3O^+) ions react with acetate (CH_3COO^-) ions and pH of the solution increase. However, the total amount of particles (atoms, ions, and molecules) increases. When the amount of solute increases, the interactions between solute particles and solvent particles increase. This causes the increase in the fluid's internal resistance to flow, which is identified as viscosity of the solution. If metal acetates are added to the solution, the total amount of electrolyte increases. The increase in amount of electrolyte causes an increase in electrical conductivity of the solution up to a certain value.

Fig. 1 exhibits a comparison between the FTIR-ATR absorbance spectra of the electrospun fibers of the PVA/Zn and the calcined undoped, Mg doped ZnO samples at 600 °C. O–H stretching appears as a broad band between 3600 and 3200 cm^{-1} while the bending appears at 1500 cm^{-1}. The existence of these bands indicated the existence of absorbed water on the surface of the electrospun nanofibers.

The intensity of the symmetry stretching at the 2920 cm^{-1} mode and the asymmetry stretching at the 2850 cm^{-1} mode of the CH_2 groups of the PVA can also be observed very clearly. A sharp band at 1090 cm^{-1} is responsible for C–O–C stretching of acetyl group present in the PVA backbone. These bands had been previously characterized by several researchers [21,22]. The 1360 cm^{-1} band and the 1440 cm^{-1} band associated with MgO [23–26] were also observed on the Mg doped ZnO samples. After the calcination, all these strong features disappeared. No sign of absorbed water or hydroxyl, carbonate, or hydrocarbon impurity could be observed.

The new peaks formed after the calcinations of the PVA/Zinc and the magnesium acetate composite electrospun fibers at 600 °C. A broad peak appeared around 605 cm^{-1} representing the M–O stretching of the MgO in the PVA backbone and the Mg doped calcined samples. The intensity of this peak went up with an increase in the Mg doping concentration. This confirmed the Mg doping of the nano ZnO composite formation.

SEM micrographs of Mg acetate loaded PVA/Zn acetate nanofibers differing in their percentage by weight are shown in Fig. 2(a–d). The average fiber diameters of the undoped PVA/Zn acetate and the Mg acetate loaded PVA/Zn acetate

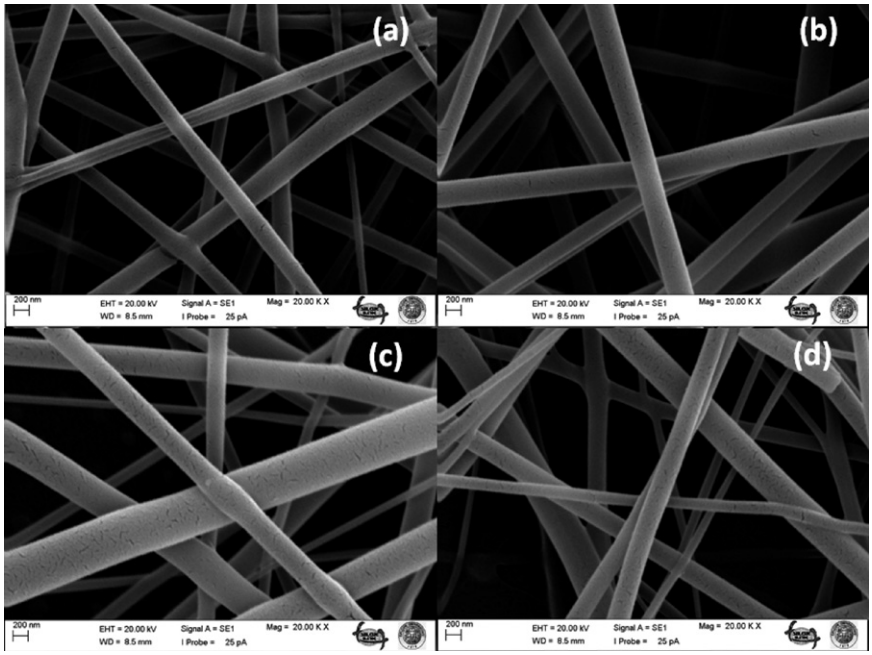

Fig. 2. SEM micrographs of the electrospun nanofibers (a) PVA/Zn acetate, (b) PVA/(Zn–%2 Mg) acetate, (c) PVA/(Zn–%4 Mg) acetate, (d) PVA/(Zn–%6 Mg) acetate nanofibers.

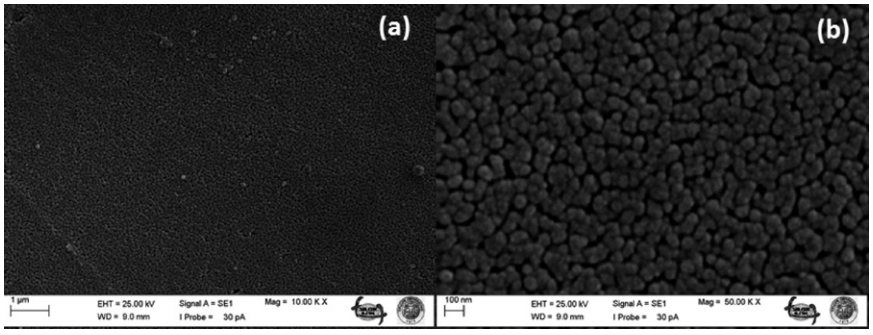

Fig. 3. SEM micrographs calcined nanoceramic mats of the PVA/(Zn–%2 Mg) Mg doped ZnO nanostructures at 600 °C.

electrospun nanofibers weighting 2%, 4% and 6% respectively were calculated for each electrospun nanofiber sample by averaging 50 fibers from the SEM images using ImageJ software as 223 nm, 213 nm, 205 nm and 176 nm, respectively.

ImageJ is a Java-based public domain program which contains basic digital image processing tools and includes numerous tools that facilitate quantitative measurements which was originally developed at the National Institutes of Health (NIH) [20]. It could be seen that all the electrospun nanofibers were linear, smooth and uniform. Moreover, the distributions of nanofibers were fairly random with no beading and distinct alignment.

Fig. 3(a) and (b) shows the calcined nanoceramic mats of the PVA/(Zn–%2 Mg) acetate nanofibers with different magnification at 600 °C. It can be seen from the SEM image that the nanofiber morphology of the electrospun fibers after the removal of the PVA component from the fibers and the conversion of metal acetates to metal oxides at 600 °C changed so that the fibers appear to consist of homogeneously distributed and perfectly linked particles or crystallites.

Fig. 4 shows the PL spectra of the undoped and the Mg doped as-synthesis PVA–ZnO composite nanofiber and the ZnO nanoparticle at room temperature. In this figure, No: 1, 2, 3 and 4 represent the undoped and the Mg doped ZnO nanofibers with the ratio of 2%, 4% and 6%, respectively. In addition, every curve in the boxes corresponds to the undoped and calcined structures at 300 °C, 400 °C, 500 °C and 600 °C respectively. As it can be seen in these figures, the ZnO nanoparticle structure was obtained after 400 °C.

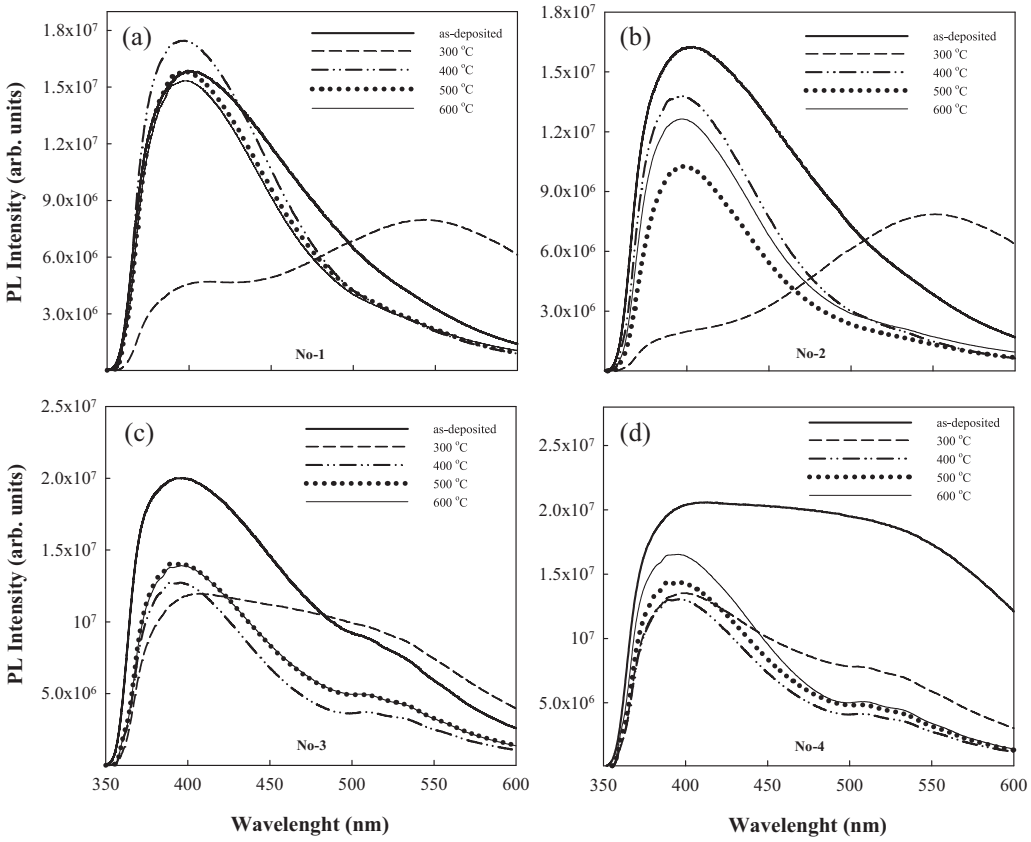

Fig. 4. The PL spectra of undoped (No-1) and Mg-doped ZnO nanofiber films with as-synthesis which was calcined at different temperatures. 2%, 4% and 6% Mg-doping by weight is shown in No-2, No-3 and No-4.

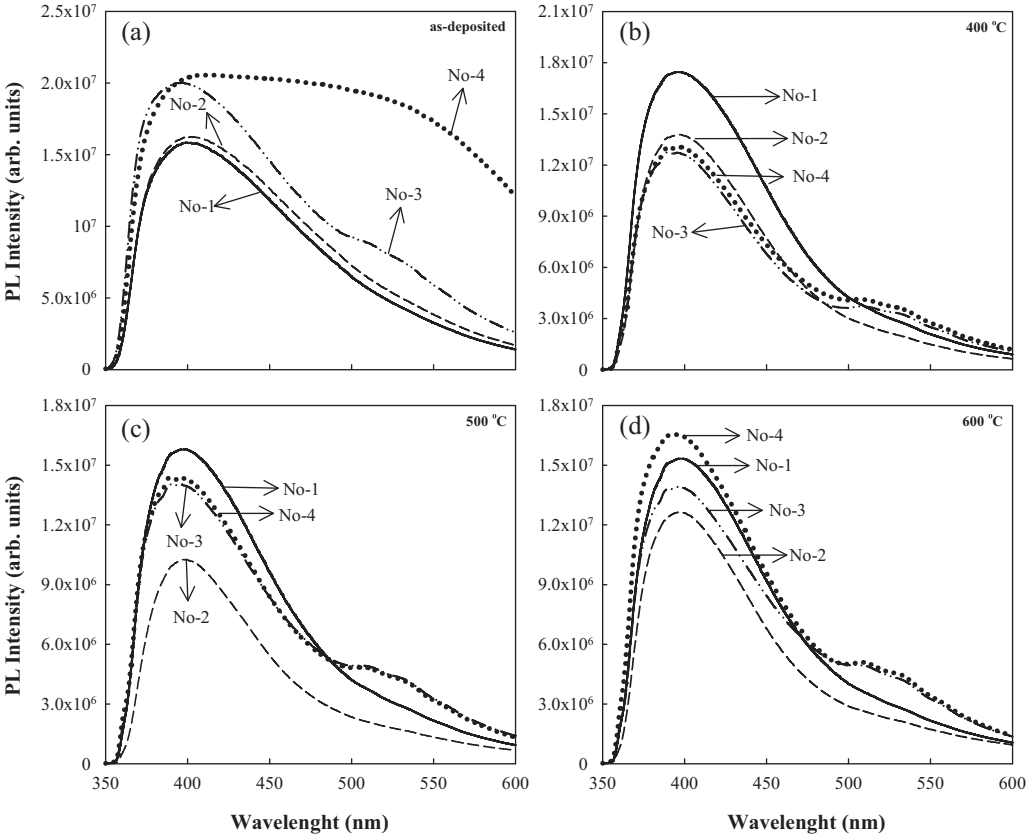

Fig. 5. The PL spectra of the undoped and Mg doped ZnO nanofibers at the same temperature.

In the PL spectra of these structures two emission peaks were observed. The main peak, located at 395 nm (3.14 eV), is attributed to the near band edge emissions (NBE) of the ZnO. Intensities of the NBE peak for the undoped structure had a maximum value at the calcining temperature of 400 °C while at the other temperatures they had approximately the same intensity. The intensity of the NBE peak of the 2% Mg-doped sample also had a maximum value at 400 °C while the intensity was decreased when the calcining temperature was increased. Contrary to this, the NBE peak intensity for the samples with the Mg-doped 4% and 6% had a maximum at 600 °C. The second broad emission peak corresponded to the defect level emission in the band gap region (deep-level transitions) which was observed in the blue–green–yellow regions. The broad deep-level emissions in the undoped ZnO nanostructure were due to the oxygen and zinc vacancy and also their interstitial related defect levels [27,28]. Related emissions with these types of defects were dominant in the case of sample 3 and sample 4. When the Mg substituted in the nanostructure, the deep-level transition peak intensity was increased by increasing the Mg doping ratio. As seen in Fig. 4(c), in the case of 6% doping ratio, deep-level emission had the highest intensity. However, the weak defect emission intensity was observed for the ZnO nanostructure with 2% Mg doping concentration at all the calcination temperatures as seen in Fig. 4(b).

The PL spectra of the nanostructure ZnO with a different doping amount of the Mg was given in same figure (Fig. 5) with the same calcination temperature for comparison. Fig. 5(a) shows that the as-synthesis ZnO nanocomposite fiber with 6% Mg-doping had a higher defect level than the others. The undoped and the 2% Mg doped composite fiber structures had nearly the same deep-level defect states. As it can be seen in Fig. 5(a–d), the PL emission peak of doped-ZnO nanostructure blue-shifted to a higher energy compared to the pure ZnO (No: 1) film. In other words the NBE peak position of the ZnO nanostructure can be slightly changed with the Mg doping ratio. For example, the shifting value of the NBE emission peak position for the undoped and the Mg(6%)-doped ZnO structure was 5 nm (4 meV). This can be explained by the modulation of the band-gap by the Mg substitution [10]. As a result of the evaluation of the PL emission of the samples, it can be said that the Mg-doped ZnO nanostructure with the doping concentration of 2% has the lowest deep-level defect center at all temperature. However, the structure with a doping concentration of 6% (No. 4) has the highest NBE emission at 600 °C and the higher defect center compared to the other samples.

The schematic representation of the energy transition mechanism from the exitonic and the defect states in the undoped and the Mg doped ZnO nanostructures is shown in Fig. 6. It is known that the undoped ZnO has an n-type doping profile. When the structure was doped with Mg, the exitonic transition energy blue-shifted to a high energy value. During the formation of the Mg:ZnO structure, Mg^{2+} ions were substituted for the Zn^{2+} ions without changing the ZnO structure. However, Mg doping in the ZnO acts as donor and the band gap energy of the structure increases. This increasing or the shifting is known

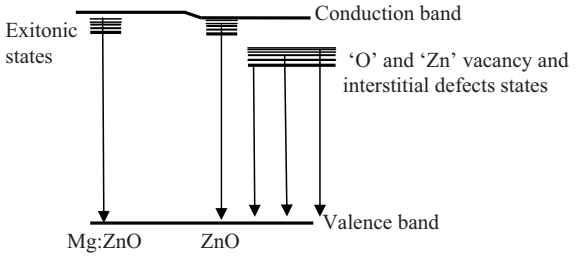

Fig. 6. The schematic representation of the energy transition mechanism in the undoped and the Mg doped ZnO nanostructures.

as Burstein Moss (BM) shift. The blue-shifting of the emission for the present samples may be explained with BM effect [29,30].

In addition, Mg(2%) doped ZnO electrospun nanofiber samples were calcined in between 300 °C and 400 °C by 20 °C steps. In order to evaluate their decomposition temperature, the emission spectra of each sample is presented in Fig. 7. The behavior of the emission spectra of the sample calcined at 300 °C is different from that of the others and has a main peak at 550 nm. The emission spectra of all the other samples have the same form and have an approximate main peak at 400 nm. This change in the behavior of the emission spectra shows that the decomposition of electrospun nanofibers starts at 320 °C.

At 320 °C and 340 °C, it can be observed that the PL peak intensity around 400 nm increases whereas the peak intensity at 550 nm drops. This situation shows that although the metal acetate structure of the electrospun nanofibers decomposes, it does not decompose completely. Calcination temperatures higher than 360 °C caused a drop in the peak at 550 nm to the lowest intensity and increased peak intensity around 400 nm. This situation can be regarded as an indication of the removal of all organic components from the electrospun nanofibers and the transformation of the structure into the Mg–ZnO form resulting from the calcination made at 360 °C. The highest peak intensity at 400 nm belongs to the sample calcined at 400 °C, therefore it can be said that it has a lower defect level.

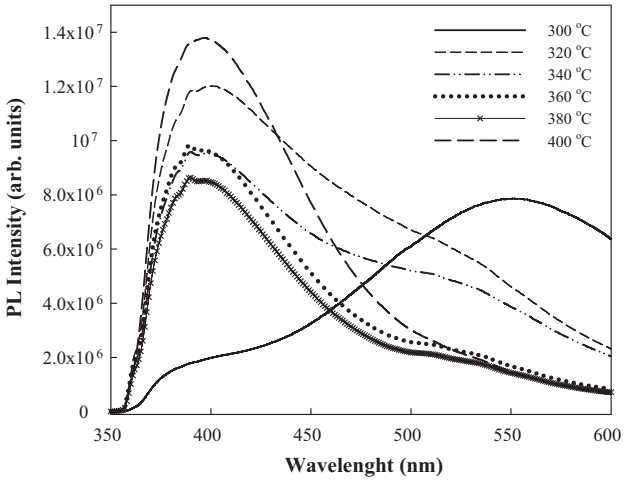

Fig. 7. The PL emission spectra of the as-synthesis ZnO nanocomposite and the Mg(2%) doped ZnO nanostructure at the calcination temperature from 300 °C to 400 °C.

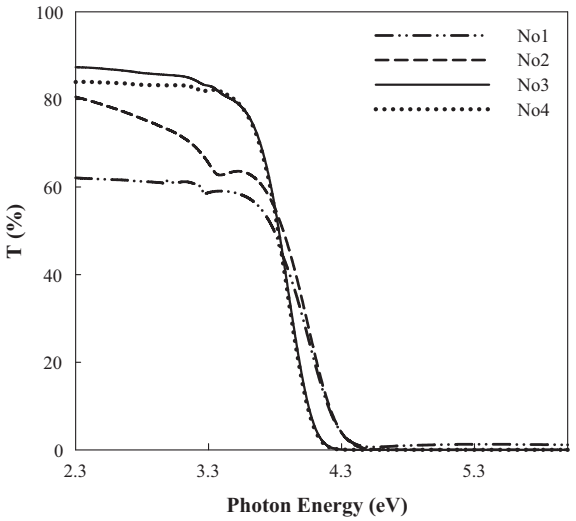

Fig. 8. The transmittance spectra of the undoped and the doped ZnO nanostructures calcined at 600 °C.

For understanding the band gap energy of the semiconductor structures, the evaluation of the optical absorption spectra is an efficient method. As known, the relationship between the optical absorption coefficient (α) and band gap (E_g) is shown as $\alpha h\nu = B(h\nu - E_g)^n$. B is a constant, $h\nu$ is the incident photon energy, and n takes on different values such as $n = 1/2$ and 2 for direct allowed transition and indirect transition, respectively [31]. Due to ZnO is a semiconductor with a direct band gap [32], n is 1/2 and $(\alpha h\nu)^2 = B(h\nu - E_g)$ [33]. The optical band gap can determined by linear fitting to linear region of the plots of $(\alpha h\nu)^2$ versus $h\nu$. In this method, when $(\alpha h\nu)^2 = 0$, the point that intersects the $h\nu$ axis corresponds to band gap energy. The transmittance spectra of our samples are presented in Fig. 8.

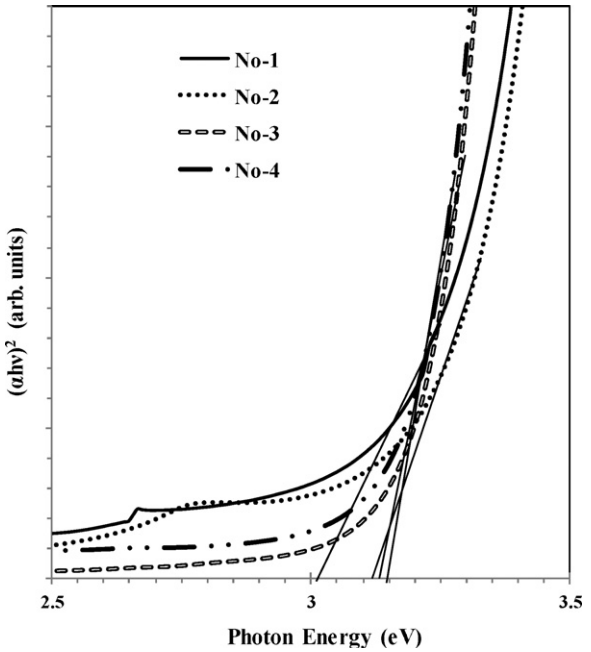

Fig. 9. The UV–VIS absorption spectra ($(\alpha h\nu)^2$ vs photon energy $h\nu$) for the undoped and Mg doped ZnO nanostructures calcined at 600 °C.

The transmission in the visible range of the Mg doped ZnO nanostructure is about 80–90%. In addition, the UV–VIS absorbency properties of the samples are presented in Fig. 9. The strong UV absorption was observed in all the samples. The band gap transitions (E_g) of the ZnO nanostructures were calculated by linear fitting to the linear region of the absorption spectra in Fig. 9. The values of E_g for the undoped ZnO acetate fiber and the Mg doped ZnO nanostructure with the ratios of 2%, 4% and 6% calcined at 600 °C were obtained as 3.03 eV, 3.12 eV, 3.13 eV and 3.15 eV, respectively. Resembling the UV emission in the PL spectra, the value of E_g for the samples was blue-shifted by increasing the Mg content in the structure as it can be seen in Fig. 9.

Also, the new electronic states were revealed between the valence band and the conduction band of the ZnO when the Mg ion was incorporated into the ZnO lattice as it can be seen in Fig. 6. Due to these defect states, the ZnO structure was able to absorb visible light. In our samples, the visible range emissions appeared in blue together with green and yellow regions from the PL spectra in Fig. 5 and the UV–VIS absorption spectra in Fig. 9. The ZnO nanostructures with 4% and 6% Mg doping have different colors due to the fact that they have more visible PL emission than the ones with 2% Mg-doping.

4. Conclusion

Mg doped ZnO acetate nanofibers with different doping concentrations were synthesized using the electrospinning technique. The SEM measurements indicate that Mg doping causes a slight decrease in the diameter of the ZnO nanofibers. The room temperature PL spectrum of all the samples included two emission peaks: a strong ultraviolet emission and a weak blue emission. The ultraviolet emission peaks blue-shifted with an increase in the Mg doping concentration. Resembling the UV emission in the PL spectra, the value of E_g for the samples blue-shifted with an increase of the Mg content in the structure. In addition, the decomposition temperature of the ZnO electrospun nanofibers into the ZnO nanoparticle structure was determined by the evaluation of the emission spectra of the samples as 320 °C.

Acknowledgement

This research was supported by state Planning Organization (DPT) by contract number 2011K120290.

References

[1] D.R. Clarke, Varistor ceramics, Journal of the American Ceramic Society 82 (1999) 485–502.
[2] M. Matsuoka, Nonohmic properties of zinc oxide ceramics, Japanese Journal of Applied Physics 10 (1971) 736–746.
[3] K. Mukae, K. Tsuda, I. Nagasawa, Non-ohmic properties of ZnO–rare earth metal oxide–Co_3O_4 ceramics, Japanese Journal of Applied Physics 16 (1977) 1361–1368.
[4] H. Ohta, K. Kawamura, M. Orita, M. Hirano, N. Sarukura, H. Hosono, Current injection emission from a transparent p–n junction composed of p-$SrCu_2O_2$/n-ZnO, Applied Physics Letters 77 (2000) 475–477.
[5] D.M. Bagnall, Y.F. Chen, Z. Zhu, T. Yao, S. Koyama, M.Y. Shen, T. Goto, Optically pumped lasing of ZnO at room temperature, Applied Physics Letters 70 (1997) 2230–2232.
[6] B.-H. Lee, S.-M. Kang, Properties of ZnO varistor blocks under multiple lightning impulse voltages, Current Applied Physics 6 (2006) 844–851.
[7] T. Makino, N.T. Tuan, H.D. Sun, C.H. China, Y. Segawa, M. Kawasaki, A. Ohotomo, K. Tamura, T. Suemoto, H. Akiyama, M. Baba, T. Tomita, H. Koinuma, Temperature dependence of near ultraviolet photoluminescence in ZnO/(Mg, Zn)O multiple quantum wells, Applied Physics Letters 78 (2001) 1979–1981.
[8] J.A. Park, J. Moon, S.J. Lee, S.C. Lim, T. Zyung, Fabrication and characterization of ZnO nanofibers by electrospinning, Current Applied Physics 9 (2009) S210–S212.
[9] J. Lee, A.J. Easteal, U. Pal, D. Bhattacharyya, Evolution of ZnO nanostructures in sol–gel synthesis, Current Applied Physics 9 (2009) 792–796.
[10] M. Zhao, X. Wang, L. Ning, H. He, J. Jia, L. Zhang, X. Li, Synthesis and optical properties of Mg-doped ZnO nanofibers prepared by electrospinning, Journal of Alloys and Compounds 507 (2010) 97–100.
[11] B. Liu, H.C. Zeng, Hydrothermal synthesis of ZnO nanorods in the diameter regime of 50 nm, Journal of American Chemical Society 125 (2003) 4430–4431.
[12] M. Guo, C.Y. Yang, M. Zhang, Y.J. Zhang, T. Ma, X.D. Wang, X.D. Wang, Effects of preparing conditions on the electrodeposition of well-aligned ZnO nanorod arrays, Electrochimica Acta 53 (2008) 4633–4641.
[13] T. Makino, C.H. Chia, N.T. Tuan, H.D. Sun, Y. Segawa, M. Kawasaki, A. Ohtomo, K. Tamura, H. Koinuma, Room-temperature luminescence of excitons in ZnO/(Mg, Zn)O multiple quantum wells on lattice-matched substrates, Applied Physics Letters 77 (2000) 975–977.
[14] A.K. Sharma, J. Naryana, J.F. Muth, C.W. Teng, C. Jin, A. Kvit, R.M. Lkolbas, O.W. Holland, Optical and structural properties of epitaxial $Mg_xZn_{1-x}O$ alloys, Applied Physics Letters 75 (1999) 3327–3329.
[15] N. Sangkhaprom, P. Supaphol, V. Pavarajarn, Fibrous zinc oxide prepared by combined electrospinning and solvothermal techniques, Ceramics International 36 (2010) 357–363.
[16] S. Hwangbo, Y.-J. Lee, K.-S. Hwang, Photoluminescence of ZnO layer on commercial glass substrate prepared by sol–gel process, Ceramics International 34 (2008) 1237–1239.
[17] H. Chen, J. Ding, S. Ma, Violet and blue-green luminescence from Ti-doped ZnO films deposited by RF reactive magnetron sputtering, Superlattices and Microstructures 49 (2011) 176–182.
[18] H. Liu, H. Qiu, X. Chen, M. Yu, M. Wang, Structural and physical properties of ZnO:Al films grown on glass by direct current magnetron sputtering with the oblique target, Current Applied Physics 9 (2009) 1217–1222.
[19] T. Terasako, M. Yagi, M. Ishizaki, Y. Senda, H. Matsuura, S. Shirakata, Growth of zinc oxide films and nanowires by atmospheric-pressure chemical vapor deposition using zinc powder and water as source materials, Surface and Coatings Technology 201 (2007) 8924–8930.
[20] http://rsbweb.nih.gov/ij/docs/intro.html.
[21] H.S. Jung, J.K. Lee, J.Y. Kim, K.S. Hong, Crystallization behaviors of nanosized MgO particles from magnesium alkoxides, Journal of Colloid and Interface Science 259 (2003) 127–132.
[22] F. Meshkani, M. Rezaei, Facile synthesis of nanocrystalline magnesium oxide with high surface area, Powder Technology 196 (2009) 85–88.
[23] G.-H. Ning, X.-P. Zhao, J. Li, Structure and optical properties of $Mg_xZn_{1-x}O$ nanoparticles prepared by sol–gel method, Optical Materials 27 (2004) 1–5.
[24] Y. Gu, D. Chen, X. Jiao, F. Liu, $LiCoO_2$–MgO coaxial fibers: co-electrospun fabrication, characterization and electrochemical properties, Journal of Materials Chemistry 17 (2007) 1769–1776.
[25] C. Shao, H. Guan, Y. Liu, R. Mu, MgO nanofibres via an electrospinning technique, Journal of Materials Science 41 (2006) 3821–3824.
[26] X. Qiu, L. Li, J. Zheng, J. Liu, X. Sun, G. Li, Origin of the enhanced photocatalytic activities of semiconductors: a case study of ZnO doped with Mg^{2+}, Journal of Physical Chemistry C 112 (2008) 12242–12248.
[27] B. Lin, Z. Fu, Y. Jia, Green luminescent center in undoped zinc oxide films deposited on silicon substrates, Applied Physics Letters 79 (2001) 943–945.

[28] S.A.M. Lima, F.A. Sigoli, M. Jafelicci Jr., M.R. Davolos, Luminescent properties and lattice defects correlation on zinc oxide, International Journal of Inorganic Materials 3 (2001) 749–754.
[29] D.T. Kim, K.S. Yu, W.T. Kim, C.D. Kim, H.L. Park, Observation of Burstein–Moss shift in heavily copper-doped phosphor, Journal of Materials Science Letters 11 (1992) 886–887.
[30] B. Karthikeyan, T. Pandiyarajan, Simple room temperature synthesis and optical studies on Mg doped ZnO nanostructures, Journal of Luminescence 130 (2010) 2317–2321.
[31] S. Kumar, V. Gupte, K. Sreenivas, Structural and optical properties of magnetron sputtered $Mg_xZn_{1-x}O$ thin films, Journal of Physics: Condensed Matter 18 (2006) 3343–3354.
[32] S. Fujihara, Y. Ogawa, A. Kasai, Tunable visible photoluminescence from ZnO thin films through Mg-doping and annealing, Chemistry of Materials 16 (2004) 2965–2968.
[33] N.F. Mott, E.A. Davis, Electronic Process in Non-crystalline Materials, Clarendon Press, Oxford, 1979.